Local structure of amorphous $Ag_5In_5Sb_{60}Te_{30}$ and In_3SbTe_2 phase change materials revealed by X-ray photoelectron and Raman spectroscopic studies

Smriti Sahu, Anbarasu Manivannan, Habibuddin Shaik, and G. Mohan Rao

Citation: Journal of Applied Physics **122**, 015305 (2017); doi: 10.1063/1.4991491
View online: http://dx.doi.org/10.1063/1.4991491
View Table of Contents: http://aip.scitation.org/toc/jap/122/1
Published by the American Institute of Physics

Local structure of amorphous $Ag_5In_5Sb_{60}Te_{30}$ and In_3SbTe_2 phase change materials revealed by X-ray photoelectron and Raman spectroscopic studies

Smriti Sahu,[1] Anbarasu Manivannan,[1,2,a)] Habibuddin Shaik,[3] and G. Mohan Rao[4]
[1]*Discipline of Electrical Engineering, Indian Institute of Technology Indore, Indore 453552, India*
[2]*Metallurgical Engineering and Materials Science, Indian Institute of Technology Indore, Indore 453552, India*
[3]*Center for Nanomaterials and MEMS, Nitte Meenakshi Institute of Technology, Yelahanka, Bangalore 560064, India*
[4]*Department of Instrumentation and Applied Physics, Indian Institute of Science, Bangalore 560012, India*

(Received 2 May 2017; accepted 20 June 2017; published online 6 July 2017)

Reversible switching between highly resistive (*binary "0"*) amorphous phase and low resistive (*binary "1"*) crystalline phase of chalcogenide-based Phase Change Materials is accredited for the development of next generation high-speed, non-volatile, data storage applications. The doped Sb-Te based materials have shown enhanced electrical/optical properties, compared to Ge-Sb-Te family for high-speed memory devices. We report here the local atomic structure of as-deposited amorphous $Ag_5In_5Sb_{60}Te_{30}$ (AIST) and In_3SbTe_2 (IST) phase change materials using X-ray photoelectron and Raman spectroscopic studies. Although AIST and IST materials show identical crystallization behavior, they differ distinctly in their crystallization temperatures. Our experimental results demonstrate that the local environment of In remains identical in the amorphous phase of both AIST and IST material, irrespective of its atomic fraction. In bonds with Sb (~44%) and Te (~56%), thereby forming the primary matrix in IST with a very few Sb-Te bonds. Sb_2Te constructs the base matrix for AIST (~63%) along with few Sb-Sb bonds. Furthermore, an interesting assimilation of the role of small-scale dopants such as Ag and In in AIST, reveals rare bonds between themselves, while showing selective substitution in the vicinity of Sb and Te. This results in increased electronegativity difference, and consequently, the bond strength is recognized as the factor rendering stability in amorphous AIST. *Published by AIP Publishing.* [http://dx.doi.org/10.1063/1.4991491]

I. INTRODUCTION

Ever since the discovery of reversible switching, known to occur from a highly resistive state (amorphous) to conductive state (crystalline) in chalcogenide materials, rigorous investigations have been carried out for novel high-speed storage devices and re-configurable electronics.[1–6] Analogous to electronic switching, the phase change was also accompanied by a sharp change in optical transmission and reflection.[7,8] Such large contrast in optical properties originating from light-induced transition, is exploited in various state-of-the-art memory products.[2,9–11] Such progressive studies were already demonstrated on various attributes such as high speed, high density, non-volatile Phase Change Memory (PCM) optical disks, which include compact disk (CD), digital versatile disk (DVD), and Blu-ray disk (BD) by employing different families of phase change (PC) materials.[12] $Ge_2Sb_2Te_5$ is one of the most reliable material used as an active layer in various optical storage discs.[13–15] In addition, a promising compound in the second family of PC materials, known as Ag, In-doped Sb_2Te (AIST), having an improved crystallization temperature (T_c) of ~165 °C, was widely used in re-writable DVDs and BDs.[2,16–18] In the same quest of novel materials with enhanced properties, In_3SbTe_2 (IST) was studied, which reveals similar crystallization behavior as compared to AIST, but possesses higher T_c above 250 °C.[6,19–21]

Although AIST and IST materials share many properties in common such as rapid crystallization, metallic crystalline nature, single phase transition, etc., they possess very different average valence p-electron count (N_P) and also different T_c, which is responsible for better data retention.[17] Moreover, IST has shown exceptional capabilities for multi-bit PCM applications.[22] Hence, both the materials have distinctly been validated as some of the best PC materials. Therefore, owing to their technological importance, a better understanding of the local structure of amorphous phase is essential.

Hence, this study aims to elucidate structural insights of as-deposited thin amorphous AIST and IST films using X-Ray Photoelectron Spectroscopy (XPS) and Raman Spectroscopy. These results demonstrate that AIST is composed of a peculiarly large fraction of Sb_2Te amidst the mutually independent small-scale dopants such as Ag and In bonds to each of the individual species. The IST is observed to be largely comprised of In-Sb and In-Te bonds with a very few Sb-Te bonds.

II. EXPERIMENTAL

DC magnetron sputtering system was employed to fabricate amorphous AIST, IST thin films using single stoichiometric $Ag_5In_5Sb_{60}Te_{30}$ and In_3SbTe_2 targets. The films were deposited on SiO_2 substrates at room temperature under rotation of 10 rpm to achieve uniform film growth. During deposition, the chamber's ambiance was maintained at 20 sccm flow rate of Argon gas. The amorphous nature of as-deposited

a)Electronic mail: anbarasu@iiti.ac.in

samples was confirmed using X-Ray diffraction, and the film thicknesses were measured using Scanning Electron Microscope (SEM, *Quanta 200, FEI*).

SPECS GmbH X-ray photoelectron spectrometer (Phoibos 100 MCD Energy Analyzer) using Mg K_α (1253.6 eV), working at 0.1 eV resolution, was employed for the XPS analysis of the as-deposited amorphous AIST and IST films. Prior to the actual recording of the spectra, the surface of all the samples was etched for few nm using an inbuilt sputter gun inside the chamber in order to remove thin oxide layer and other adsorbed contaminants. All the spectra are charge corrected using C 1s peak as the reference for individual scans that was recorded before and after each scan for the characteristic elements. The atomic compositions were found to be $Ag_4In_7Sb_{63}Te_{26}$ and $In_{45}Sb_{19}Te_{36}$ within 5 at. % variations as measured by XPS spectral quantitative analysis. Deconvolution of the XPS spectra was performed as per requirement, using *XPS Peak 4.1* software. The fitting function Pseudo-Voigt (convolution of Gaussian and Lorentzian function) was used, and the background reduction was Shirley + Linear for all the deconvolutions. For peaks with multiplet splitting (type "p," "d," and "f"), the full width half maximum (FWHM) of the two split parts (3/2 and 5/2) were kept equal, and the typical spin-orbital splitting was fixed prior to optimization of fitting.

In order to record the Raman spectra, LabRAM *HR* model of Horiba Jobin Yvon's High-Resolution Raman Microspectrometer was used. As-deposited amorphous films having a thickness of 100 nm were utilized. The excitation wavelength for all the measurements was 632.8 nm with a spot size of 1 μm using 100× objective and a spectral resolution of 0.6 cm^{-1} at room temperature in air. The power and integration time of laser excitation was carefully optimized in order to avoid laser induced heating and phase change in the amorphous material due to exposure. To comprehend the spectra effectively, they were deconvoluted by fitting Gaussian peaks as assigned Raman modes.

III. RESULTS AND DISCUSSION

As per the stoichiometry of the two specimen films, it is evident that In along with Ag in AIST acts only as small-scale dopants in the host matrix of Sb_2Te. Although the crystalline structure of AIST was thoroughly studied,[17,18,22,23] the amorphous phase was poorly understood. On the other hand, IST is a composition along the pseudobinary tie-line of InSb and InTe,[19] whose amorphous phase is proposed to be a mixture of InSb and InTe with very few Sb-Te bonds as proposed, based on *ab initio* molecular dynamics simulation and microscopic studies.[24–26] However, till date, there are very few experimental studies primarily focusing on the local atomic structure of amorphous IST PC material.[27] Such information would immensely be helpful towards understanding thermal stability, crystallization, mechanism and speed, detectable and usable *off*-state resistance that are subject to local structure and bonding in the amorphous phase. Conceding to this fact, we present here the chemical binding states of individual species with the neighboring environment in the as-deposited amorphous phase using XPS and Raman spectroscopy. All the XPS peaks are analyzed based on the comparison with the National Institute of Standards and Technology (NIST) XPS Database, Version 4.1.[28]

A. XPS and Raman spectra of AgInSbTe

Figures 1(a)–1(d) display the 3d core level XPS spectra of as-deposited AIST of all the four individual species namely Ag, In, Sb, and Te. Appropriate deconvolution was performed to segregate the contribution from oxide groups (if any) primary lattice components. As the affinity of Ag towards O is significantly high, it is more vulnerable to become oxidized, due to which, in Fig. 1(a), one could observe a large presence of silver oxide. Yet, Ag-Ag and Ag-Te bonds can be clearly identified from the 3d spectra. No photoelectron emissions emerge from Ag-Sb species, and hence, it is difficult to comment on their presence solely on the basis of the core level spectra. Further, In 3d detailed spectra is given in Fig. 1(b) that shows a clear dominance of In-Te and In-Sb bonds. Moreover, both InTe and In_2Te_3 compositions are present in the amorphous sample, with the latter having slightly lesser intensity peak.

Ag and In acts as dopants in the primary Sb_2Te matrix to form AIST. This quotes Sb as the most dominant species in AIST, and hence, core level peak at 528.05 eV in Fig. 1(c), observed without any measurable shift in binding energy, is assigned to the Sb-Sb bonds. Moreover, some of the reports[29] suggest that this peak is primarily originating from In-Sb bonds, which could be possibly taken into consideration due to the presence of InSb peaks in 3d spectra of In and also $InSbO_x$ in Sb. The Te 3d spectra in Fig. 1(d) involve the contribution from In-Te bonds, forming InTe and In_2Te_3, in conformance with that seen in In 3d spectra. Also, Ag-Te peak could be noticed at the asymmetrically shaped side owing to atomic oscillations produced by a part of photon energy delivered during excitation. The information regarding Sb-Te bonds could not be extracted based on the study of 3d core level spectra, and also the presence of O 1s peak hinders the analysis of bonds in Sb 3d spectra. Thus, we deconvoluted and analyzed the Sb 4d spectra as shown in Fig. 2. The primary matrix of Sb_2Te is strongly recognized with an overlap of In-Sb bonds and relatively fewer Sb-Sb bonds as well.

To quantify the fraction of different types of species present in the amorphous AIST sample, we calculated the ratio of the area under the curve from the fitted XPS peaks. The Sb_2Te as seen in the Sb 4d spectra is found to be predominant in the matrix about ∼63%. A smaller ratio could also be assigned to Sb-Sb bonds (with more of covalent nature), which is in conformance with the density functional molecular dynamics simulations.[17] Most importantly, the small scale dopants, Ag and In were identified as the elements incorporating stability to the amorphous phase, but the precise role was not determined.[17] As seen from Fig. 1(b), ∼55% of In atoms coordinate with Te while ∼45% with Sb. Similarly, ∼58% of Ag is deduced to be bonded with Te atoms, along with some Ag-Ag species. However, due to an extremely small difference in the electronegativity of Ag (1.93) and Sb (2.05), the shift in the binding energy of the XPS peak relating to Ag-Sb species remains undetectable. In addition, the absence of contributions from Ag-In bonds reinforce the arguments regarding their seldom

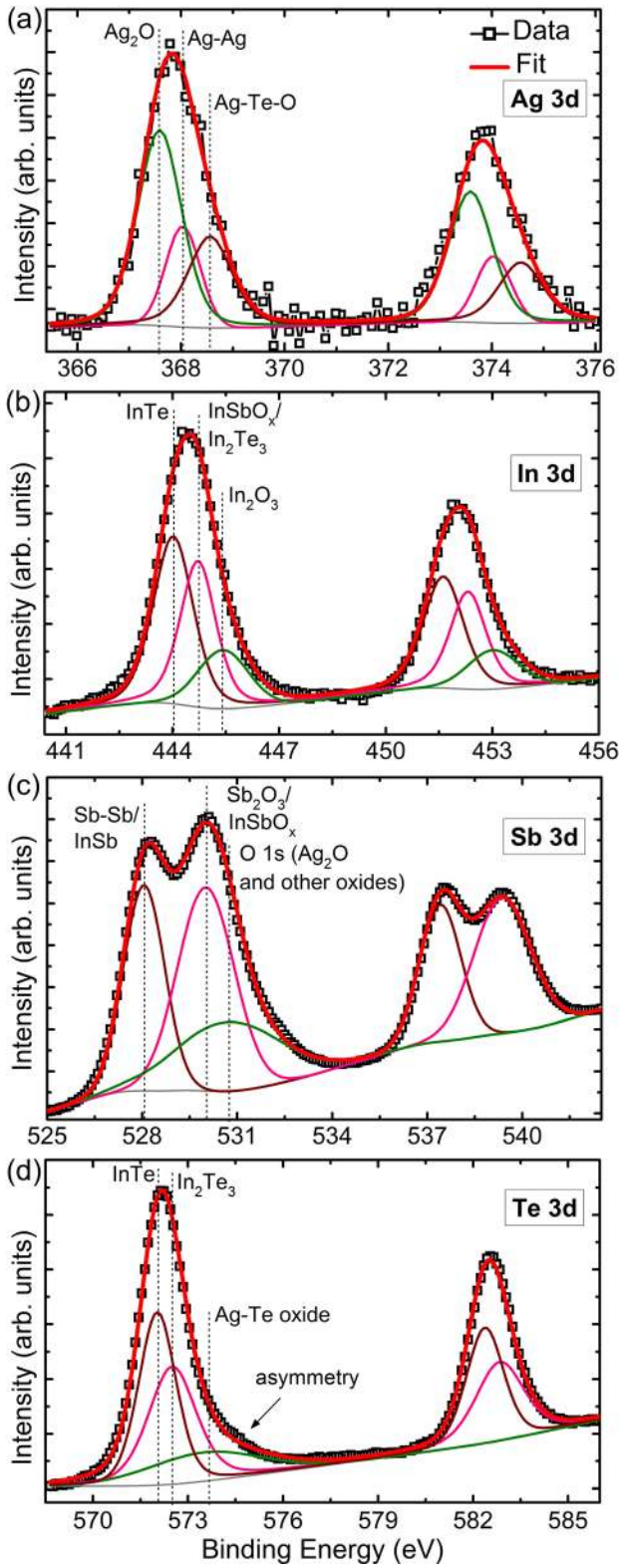

FIG. 1. XPS core level spectra of (a) Ag 3d, (b) In 3d, (c) Sb 3d, and (d) Te 3d, for as-deposited AIST.

bonding.[17] As a deduction of all XPS core level spectra, it is noteworthy to mention that in amorphous AIST, the principal matrix is composed of Sb_2Te with significant numbers of Sb-Sb bonds. The dopant In exists as In-Sb and In-Te and the dopant Ag as Ag-Te. However, bonding of Ag with Sb could not be inferred from this measurement.

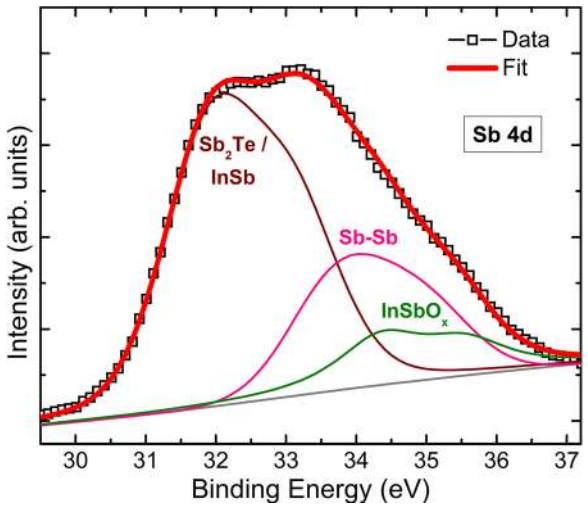

FIG. 2. XPS Sb 4d core level spectra for as-deposited AIST.

In order to validate these observations, we recorded Raman spectra on 100 nm as-deposited amorphous AIST thin film samples. The base-corrected and deconvoluted spectrum is shown in Fig. 3. The broad Raman feature, ranging from 70 to 200 cm^{-1}, is predominantly occupied by the peaks at ~92 and 141 cm^{-1} attributed to Ag-In-Te, and at ~128 and ~155 cm^{-1} representing vibrational modes of Ag-Sb-Te.[30] In addition, we can distinctly identify the vibrational modes at ~82 and 112 cm^{-1} that are corresponding to Ag-Sb.[30] This verifies the presence of Ag-Sb bonds, which were not visible from the XPS spectra as shown in Figs. 1 and 2. The mode at ~190 cm^{-1} confirms the presence of a small amount of InSb along with other substantial species in agreement with literature.[31] The Raman measurement firmly supports the contemplated contributions from XPS spectra, providing additional information on the occurrence of Ag-Sb bonds. The higher electronegativity difference between Ag-Sb, Ag-Te, In-Sb, and In-Te, as compared to Sb-Te implies an increased bond strength, and hence renders a concrete support to the findings of enhanced amorphous stability subjected to dopants Ag and In.[17]

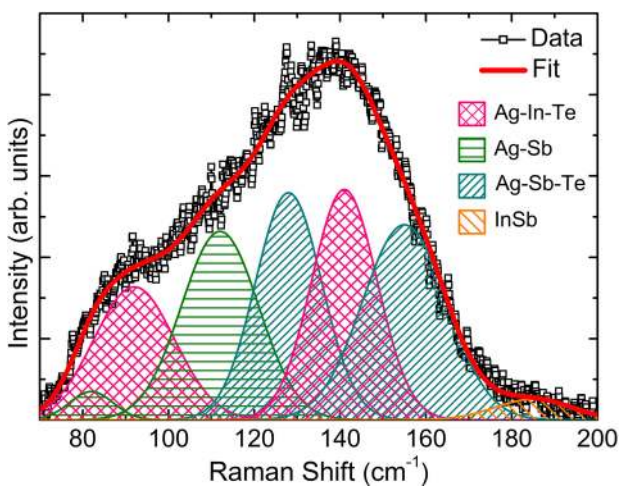

FIG. 3. Raman spectra for as-deposited AIST thin film.

B. XPS and Raman spectra of InSbTe

Strengthening the primitive presence of InSb and InTe by *ab initio* molecular dynamics simulation,[24] our experimental In 3d core level spectra presented in Fig. 4(a) unfold the bonding of dominant element (~45%), In with Sb and Te as InSb and InTe. It is noteworthy that a significant ratio of In-In bonds is also seen in the spectra that was also previously observed in the as-deposited samples of In doped SbTe.[27] Despite the fact that IST is a pseudobinary compound on the tie-line between InSb and InTe, in the present case, In_2Te_3 is seen to be dominating. A plausible explanation for this would be based on the comparison of enthalpy of formation. The enthalpy of formation of In_2Te_3 is $-(188.0 \pm 1.3)$ kJ mol^{-1} and that for InTe is $-(71.2 \pm 0.4)$ kJ mol^{-1}.[32] Hence, the probability of formation of In_2Te_3 is more than that of InTe. Since the amorphous films were made using sputtering from the single stoichiometric target, this atom-by-atom deposition favors the formation of In_2Te_3 over InTe. The calculation of fractions of different species revealed ~56% In-Te and ~44% In-Sb bonds, with a probable small hidden percentage of In-In bonds, which is in agreement with the simulation study.[24]

The Sb 3d spectrum in Fig. 4(b) is fitted with photoemission peaks from InSb at ~528.3 eV and its oxides at ~530.1 eV. Unlike Sb 3d spectra of AIST, there is no trace of the peak corresponding to Sb-Sb bonds. Figure 4(c) shows that Te 3d spectra are ubiquitously occupied by photoemission peaks from In_2Te_3 (~63%) and InTe (~37%) species, with a certainty of the presence of a small number of Te-Te bonds, as per the molecular dynamics study.[24] In addition, a comparison of normalized Te 3d spectra revealed an increase in line width by ~0.3 eV for IST over AIST, while there was precisely no change in case of In 3d spectra. This increase in spectral line width may be an indication of the increase in the randomness in the neighboring environment of Te in IST.

Consolidating the information from all 3d spectra, the as-deposited IST is exclusively composed of In-Sb and In-Te bonds, while a minority fraction of Sb-Te bonds was reported by means of density functional molecular dynamic simulation.[24] These Sb-Te bonds are considered as "wrong bonds" and homopolar pairs. Therefore, in order to investigate the presence of Sb-Te bonds, we studied the Sb 4d spectra as shown in Fig. 5. The Sb 4d spectrum is also predominantly engaged with InSb species. But, a relatively smaller set of peaks could be seen originating from Sb-Te. This confirms the presence of a small number of Sb-Te bonds in addition to InSb and InTe. Furthermore, the Sb-Sb bonds could also be assigned to a smaller volume, which is in good agreement with the previous simulation reports.[24]

The validation of peak assignments for Figs. 4 and 5 was performed using Raman spectra, and the same is shown in Fig. 6. The assertive modes were found to be at 85.7, 125.9, and 139.1 cm^{-1}, attributed to In-Te,[33,34] and a large contribution at ~105 cm^{-1}, that corresponds to In-Sb-Te.[35] Proportionately, lower volume of broad Raman spectra ranging from 70 to 200 cm^{-1}, at the higher Raman shift side,

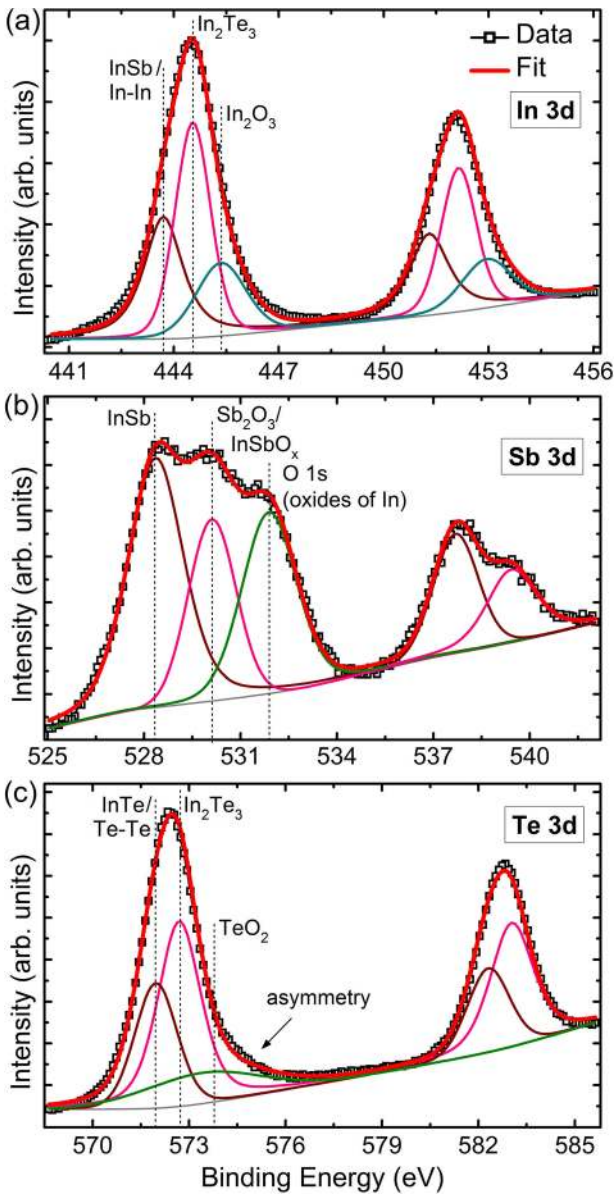

FIG. 4. XPS core level spectra of (a) In 3d, (b) Sb 3d, and (c) Te 3d, for as-deposited IST.

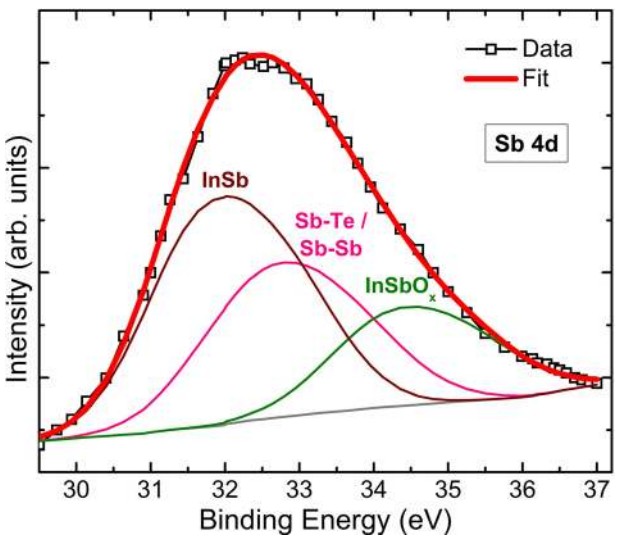

FIG. 5. XPS Sb 4d core level spectra for as-deposited IST.

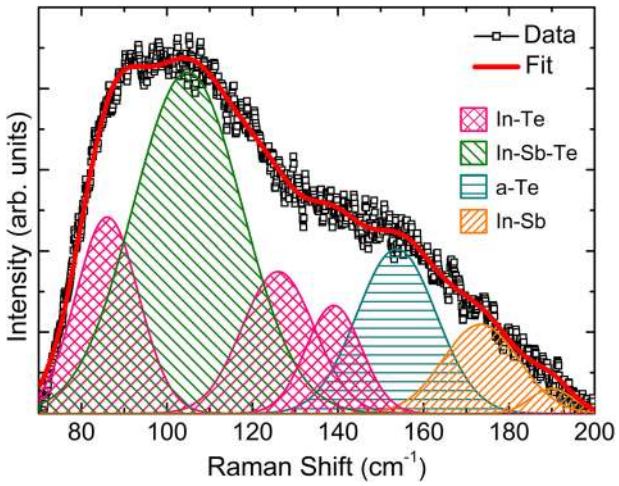

FIG. 6. Raman spectra for as-deposited IST thin film.

indicates the presence of amorphous Te at $\sim 153\,cm^{-1}$ and InSb at $\sim 180–190\,cm^{-1}$.[31,33,36] The Raman modes of IST are found to be in good agreement with the XPS photoemission peaks as discussed earlier.

The complete set of individual XPS results and Raman spectra for as-deposited amorphous AIST and IST films suggests a primary matrix involving Sb_2Te in AIST, on the other hand, In-Sb and In-Te with a very small amount of homopolar pairs of Sb-Te in IST. Additionally, Sb-Sb bonds are present in AIST in large numbers but relatively very small in IST. Furthermore, Ag and In selectively substitute some of the atoms in the vicinity of Sb and Te atoms in AIST, thereby reducing the electronegativity of the bonding neighbor.

IV. CONCLUSION

We have demonstrated a detailed analysis of XPS and Raman spectra of as-deposited amorphous AIST and IST materials. Our experimental data confirm that In is identical with its nearest neighbors, forming In-Sb and In-Te in both AIST and IST materials. The primary matrix of IST is composed of In-Sb and In-Te with very small amounts of Sb-Te and Sb-Sb, while in the case of AIST, a prime matrix of Sb_2Te with Sb-Sb is present. The Te-site of IST is observed to be disordered to a larger extent than that of AIST. The dopants of Ag and In are incorporated in the local environment of Sb and Te, leading to the reduction of neighboring atom electronegativity and consequently increasing the bond strength.

ACKNOWLEDGMENTS

A.M. is thankful to the Department of Science and Technology (Grant No. SB/EMEQ-032/2013) and the Department of Atomic Energy (Grant No. 2013/20/34/2/BRNS), Government of India, for the financial support.

[1]M. H. R. Lankhorst, B. W. S. M. M. Ketelaars, and R. A. M. Wolters, Nat. Mater. **4**, 347 (2005).
[2]M. Wuttig and N. Yamada, Nat. Mater. **6**, 824 (2007).
[3]E. T. Kim, J. Y. Lee, and Y. T. Kim, Phys. Status Solidi RRL **3**, 103 (2009).
[4]D. Loke, T. H. Lee, W. J. Wang, L. P. Shi, R. Zhao, Y. C. Yeo, T. C. Chong, and S. R. Elliot, Science **336**, 1566 (2012).
[5]W. W. Koelmans, A. Sebastian, V. P. Jonnalagadda, D. Krebs, L. Dellmann, and E. Elefteriou, Nat. Commun. **6**, 8181 (2015).
[6]S. K. Pandey and A. Manivannan, Appl. Phys. Lett. **108**, 233501 (2016).
[7]J. Feinleib, J. deNeufville, S. C. Moss, and S. R. Ovshinsky, Appl. Phys. Lett. **18**, 254 (1971).
[8]W. Welnic, S. Botti, L. Reining, and M. Wuttig, Phys. Rev. Lett. **98**, 236403 (2007).
[9]E. R. Meinders, A. V. Mijritskii, L. van Pieterson, and M. Wuttig, *Optical Data Storage: Phase Change Media and Recording* (Springer, Berlin, 2006).
[10]C. Rios, P. Hosseini, C. D. Wright, H. Bhaskaran, and W. H. P. Pernice, Adv. Mater. **26**, 1372 (2013).
[11]P. Hosseini, C. D. Wright, and H. Bhaskaran, Nature **511**, 206 (2014).
[12]D. Lencer, M. Salinga, and M. Wuttig, Adv. Mater. **23**, 2030 (2011).
[13]A. V. Kolobov, P. Fons, A. I. Frenkel, A. L. Ankudinov, J. Tominaga, and T. Uruga, Nat. Mater. **3**, 703 (2004).
[14]N. Yamada, E. Ohno, K. Nishiuchi, N. Akahira, and M. Takao, J. Appl. Phys. **69**, 2849 (1991).
[15]J. Siegel, A. Schropp, J. Solis, C. S. Afonso, and M. Wuttig, Appl. Phys. Lett. **84**, 2250 (2004).
[16]H. Iwasaki, M. Harigaya, O. Nonoyama, Y. Kageyama, M. Takahashi, K. Yamada, H. Deguchi, and Y. Ide, Jpn. J. Appl. Phys., Part 1 **32**, 5241 (1993).
[17]T. Matsunaga, J. Akola, S. Kohara, T. Honma, K. Kobayashi, E. Ikenaga, R. O. Jones, N. Yamada, M. Takata, and R. Kojima, Nat. Mater. **10**, 129 (2011).
[18]T. Matsunaga, Y. Umetani, and N. Yamada, Phys. Rev. B **64**, 184116 (2001).
[19]Y. Maeda, H. Andoh, I. Ikuta, and H. Minemura, J. Appl. Phys. **64**, 1715 (1988).
[20]Y. T. Kim and S. Kim, Appl. Phys. Lett. **103**, 121906 (2013).
[21]V. L. Deringer, W. Zhang, P. Rausch, R. Mazzarello, R. Dronskowski, and M. Wuttig, J. Mater. Chem. C **3**, 9519 (2015).
[22]H. Tashiro, M. Harigaya, Y. Kageyama, K. Ito, M. Shinotsuka, K. Tani, A. Watada, N. Yiwata, Y. Nakata, and S. Emura, Jpn. J. Appl. Phys., Part 1 **41**, 3758 (2002).
[23]J. Akola and R. O. Jones, in Proceedings of the NIC Symposium, February 2012, Julich, Germany.
[24]J. H. Los, T. D. Kuhne, S. Gabardi, and M. Bernasconi, Phys. Rev. B **88**, 174203 (2013).
[25]K. D. Flynn and D. Strand, Jpn. J. Appl. Phys., Part 1 **42**, 795 (2003).
[26]Y. T. Kim, E. T. Kim, C. S. Kim, and J. Y. Lee, Phys. Status Solidi RRL **5**, 98 (2011).
[27]M. H. Jang, S. J. Park, D. H. Lim, S. J. Park, M. H. Cho, D. H. Ko, M. Y. Heo, H. C. Sohn, and S. O. Kim, Appl. Phys. Lett. **96**, 052112 (2010).
[28]NIST X-ray Photoelectron Spectroscopy Database, Version 4.1 (National Institute of Standards and Technology, Gaithersburg, 2012); See http://srdata.nist.gov/xps/ for comprehensive information on energies of photoelectrons with the corresponding line positions and chemical shifts.
[29]D. M. Poirier and J. H. Weaver, Surf. Sci. Spectrom. **2**, 217 (1993).
[30]J. Tominaga, T. Kikukawa, M. Takahashi, and R. T. Phillips, J. Appl. Phys. **82**, 3214 (1997).
[31]A. Pinczuk and E. Burstein, Phys. Rev. Lett. **21**, 1073 (1968).
[32]E. G. Lavut, N. V. Chelovskaya, G. A. Belysheva, V. N. Demin, and V. P. Zlomanov, J. Chem. Thermodyn. **26**, 577 (1994); **29**, 43 (1997).
[33]J.-L. Battaglia, A. Kusiak, C. Gaborieau, Y. Anguy, H. T. Nguyen, C. Wiemer, R. Fallica, D. Campi, M. Bernasconi, and M. Longo, Phys. Status Solidi RRL **10**, 544 (2016).
[34]M. A. Nizametdinova, Phys. Status Solidi B **97**, K9 (1980).
[35]J. K. Ahn, K. W. Park, S. G. Hur, C. S. Kim, J. Y. Lee, and S. G. Yoon, J. Nanosci. Nanotechnol. **11**, 189 (2011).
[36]M. H. Brodsky, R. J. Gambino, J. E. Smith, Jr., and Y. Yacoby, Phys. Status Solidi B **52**, 609 (1972).